A Tunable Magnet-based Tactile Sensor Framework

Evan Harber, Evan Schindewolf, Vickie Webster-Wood, Howie Choset, and Lu Li
Robotics Institute, Carnegie Mellon University, Pittsburgh, PA, USA, 15213
email: lilu12@andrew.cmu.edu, choset@andrew.cmu.edu, vwebster@andrew.cmu.edu,

***Abstract*—Tactile sensing enables controllable interactions as robots enter unknown and unstructured environments. However, existing tactile sensors suffer from limited form factors and durability, lack of dynamic range, and are not cost-effective. Magnet-elastomer-based tactile sensors offer a potential solution to compensate for these deficiencies. In this paper, we present a generalizable design approach, a first-order model based on the magnetic field and elastomer fundamentals, and an automated calibration routine to create custom tactile sensors. To demonstrate the performance and versatility of the proposed sensor architecture, we selected two sample design configurations: a small form factor that was optimized for tumor localization (Pinky) and a larger form factor for robust contact estimation on legged robots (Foot). These two unique cases demonstrate the breadth of sensors that can be designed using this approach as well as how changes in sensor parameters can be used to tune the range and resolution for different applications.**

I. Introduction

Tactile sensing offers a unique stream of directly measured data which can allow systems to estimate and react to physical properties such as friction, stiffness, or weight distribution. Unlike approaches that rely on visual cues, tactile sensors can provide physical measurements even in environments with occluding physical barriers. The variety of applications for tactile sensors (from robotic palpation to locomotion) provides a wide range of constraints such as in form, fidelity, durability, sensing range, and cost. For example, robot-assisted minimally invasive surgery (RMIS) might set requirements for the size and resolution of the tactile sensor while sensorized robotic feet may require durability and a high dynamic range. Traditionally, strain gauges have been used to provide force feedback. However, due to their cost and overload limitations, the sensor community has started to explore the concept of soft force sensors [1]–[5].

In this paper, we aim to demonstrate the capability of a tactile sensor design based on embedding a magnet inside a soft elastomer to satisfy the above requirements. Previous work in this area has shown that this type of sensor can achieve high sensitivity and resolution in a small package [5]. With a few modifications, the proposed work is more adaptable to real world requirements such as durability and wide sensing range. We also developed a generalizable model for these embedded magnet-based force sensor along with an automated calibration process for sensor profiling. To demonstrate the versatility of this sensor framework, we present two force sensors to demonstrate the capability and customizability through potential applications of this sensor framework.

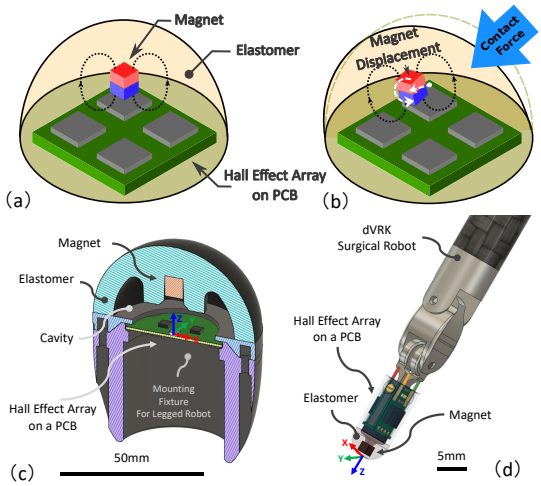

Fig. 1: Theory of operation for proposed sensor (a)(b) and two applications (c)(d). Foot Sensor (c) designed for contact mapping during robot locomotion. Pinky Sensor (d) designed for tumor stiffness mapping.

II. Sensor Design

The sensor presented in this paper, shown in Fig. 1, relies on measuring the applied force through estimating magnet displacement induced by deformation of the elastomer. The parameters in this framework that directly impact fidelity and sensing range are the magnet strength and location, cavity size, number of Hall effect sensors, elastomer durometer, and wall thickness. Elastomer durometer and wall thickness also impact durability and magnet protection. This is essential since high strength neodymium magnets, such as the ones we use (K&J Magnets, USA), are extremely brittle. Using a cubic magnet also provides the benefit of allowing for 90 degrees of sensing range about its magnetization axis, whereas continuous symmetry in cylindrical magnets makes this impossible. Capturing the magnet's six degree of freedom (DoF) pose requires an at least nine-dimensional Hall effect sensor array, three for environmental field cancellation and six for magnet pose estimation.

A. Theoretical Sensor Model

As external forces or stresses ($\vec{\sigma}$) are applied to the elastomer, the elastomer experiences a deformation or a strain ($\vec{\epsilon}$). With the magnet embedded inside the elastomer, these strains create a change in magnetic field ($\vec{B}$) which can be measured by the Hall effect sensors.

Since both the strain and magnetic field operate as a function of the magnet's pose ($\vec{r}$), a conversion between the two can be established. The magnetic field equation can generally be modeled as an inverse cubic law w.r.t. distance ($\vec{r} = O(\vec{B}^{-1/3})$) [6]. Due to the placement of the magnet embedded inside the elastomer, the strain can be found using a change in magnet pose ($\vec{\epsilon} = \Delta\vec{r}$).

Modeling the stress-strain relationship is not trivial. Elastomers are generally viscoelastic due to molecular resistance to deformation. This introduces a time dependence into this relationship usually modeled using a generalized Maxwell's model (GMM) as a series of springs and spring dampeners in parallel (Fig. 2b). Solving the resulting differential equation for a singular step input (and assuming each dimensional independence) results in a series of independent decaying exponentials [7]:

$$\vec{\sigma}(t) = f(\vec{\epsilon}) \circ [\sum_{n=1}^{N} \vec{A}_n \circ e^{-\vec{B}_n t}] \approx \vec{C} \circ f(\vec{\epsilon}) \quad (1)$$

where $f(\vec{\epsilon})$ is a linearizing function between stress and strain and $\vec{C}$ is a vector of stiffness coefficients. In practice, this introduces a small amount of error into the system, mainly due to stress relaxation or hysteresis. Some work has been done on modeling and canceling out the time dependent effect [8]. However, since it is rather complicated and introduces a time dependence into the model, this work will ignore this effect and will instead use a model based on the steady-state solution. This simplifies Eq. 1 to the linear equation, Hooke's Law. Combining this concept, along with the inverse cubic law for magnetic field, we get the following equation relating magnetic field to stress:

$$\vec{\sigma} = \vec{C} \circ f(\Delta\vec{r}) = O(\Delta\vec{B}^{-1/3}) \approx O(\vec{B}_0 - \sum_{n=0}^{\inf} \vec{C}_n \circ \vec{B}^n). \quad (2)$$

This can be expanded using classic Taylor series expansion to a sum of powers as long as the stress-strain curves can be equivalently modeled by a polynomial (Fig. 2c and Fig. 2d). We can, therefore, effectively model and calibrate the equations relating the magnetic field to the stress through a high order multi-dimensional polynomial (MDP), as shown in Eq. 2.

B. Fabrication

With mass-producibility in mind, this framework is designed with durable and low-cost materials, and for scalable fabrication techniques. The elastomer casting process includes overmolding thermoset urethane (VytaFlex, Smooth-On, USA) onto a mounting piece and 3D printed water soluble (PVA, Ultimaker, USA) positive mold of the cavity, post-curing for four hours at 65 °C, and dissolving the cavity mold in water.

After this is complete, the magnet is inserted into the cavity and fixed in place using a urethane adhesive compound (UreBond II, Smooth-On, USA) such that the magnetic field is perpendicular to the surface of the elastomer at the tip. Finally,

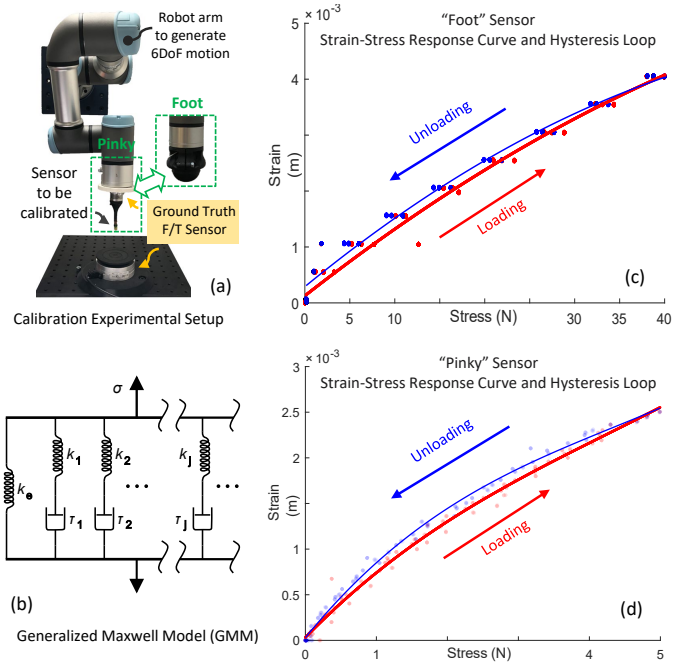

Fig. 2: The sensor benchmark and calibration setup (a) and the elastomer model (b) used for the collection of multi-axis stress-strain, contact point location, and hysteresis data (c,d) normal to the tip.

the printed circuit boards (PCB) are fixed to the mounting piece using brass screws and threaded inserts so as not to respond to magnetic fields. The PCBs are designed for each application to fit within the sensor's form factor. See Table I for further details on the Pinky and Foot sensor parameters.

TABLE I: Sensor Parameters

Sensor Parameter	**Sample Sensor Design**	
	Pinky Sensor	***Foot Sensor***
Elastomer Durometer	10A	30A
Elastomer Dome Radius (mm)	3	25.4
Elastomer Cavity	No	Yes
Elastomer Wall (mm)[a]	0.9	9.0
Magnet Size (in)	1/16	1/4
Magnet Model	B111	B444-N52
Number of Tri-axis Hall Effect Sensors	3	4

[a]Elastomer Wall is the thinnest point of the elastomer between the surface of the magnet and the exterior surface of the elastomer.

III. Experiments and Applications

A. "Foot" Sensor for impact and coarse contact estimation

Calibration and validation data sets are collected using a UR3e series robot (Universal Robots, Denmark). As seen in Fig. 2a, the robot arm is used to manipulate the force sensor and apply normal forces across the surface of the Foot sensor. Using a 1D Loadstar Force sensor (TUF-050-025-A*C01, Loadstar, USA) as ground truth, this routine creates a data set of positions ranging from approximately -15 to 15 mm as measured along a surface made by projecting the elastomer onto the hall effect sensor array with forces ranging from 0 to about 30 N. Small shear displacements of a maximum of 5 mm are also introduced at each surface Normal in order to

promote extrapolation when a limited range of shear forces are present. This data set can be used to fit the MDP model outlined in Section II. With surface geometry impacting the elastomer deformation, we have constrained both the input and validation data sets to only include contact with a flat surface. The results are summarized in Table II.

B. "Pinky" Sensor for fine measurement of 3D forces

Because the Pinky sensor is of significantly smaller size than the Foot sensor, we can treat the entirety of the force sensor as a point, which eliminates contact point localization. This sensor is trained and validated for 3 DoF (1 normal and 2 shear) forces. Similar to the previous section, we used a UR3e arm to create the training and validation data sets. By applying normal and shear forces across the tip of the Pinky sensor with a 6-DoF ATI-Nano 25 (ATI Industrial Automation, USA) as ground truth (Fig. 2a) we can similarly create a training and validation data set to be used to train and test the MDP model. The results are summarized in Table II.

TABLE II: Sensor Performance and Error Summary

Foot Sensor Benchmark[a]			**Pinky Sensor Benchmark**[b]		
Output	***Range***	***Error***	***Output***	***Range***	***Error***
Normal (N)	32.80	4.61%	Normal (N)	5.32	0.41%
Cx (mm)[c]	±15.28	22.05%	Shear-x (N)	±0.49	0.16%
Cy (mm)[c]	±15.28	21.89%	Shear-y (N)	±0.46	0.37%

Result calculated from experiment data sets containing
[a] ≈ 300,000 and [b] ≈ 8,000 samples each.
[c] Estimated contact point dome projected to the base X-Y plane

C. "Foot" Sensor Application: Contact Identification

Legged robots, with their high degree of articulation, can maneuver through unstructured environments. However, most dynamic models and controllers rely on a system that can identify the instant of foot contact as it marks a significant landmark in the gait cycle. Sensorized feet are one potential solution for the direct measurement of ground contact [9]. As opposed to measuring the change in knee acceleration or using visual features, this solution is less prone to noise and is especially beneficial for large dynamic actions (eg. stair climbing) or occluded environments (eg. walking through mud or brush). Fig. 3 demonstrates a biped walking using these principles. Outlined further in [10] this biped uses the sensorized feet to determine when to take its next step. By recognizing the moment both feet are on the ground, it switches which leg is in its stance phase and which leg should swing. In maintaining one leg in contact with the ground, the robot is able to walk over the flat ground as well as more uneven terrain.

D. "Pinky" Sensor Application: Stiff Feature Identification

Robot-assisted minimally invasive surgery (RMIS) augments the surgeon's limited sensory information and can be used to reduce cognitive load, allowing for better patient outcomes [11] [12]. One potential application is tumor stiffness mapping [13]. Fig. 4 is an example of a uniform tissue with two large solid structures (representing tumors) embedded inside. A discrete palpation process that measures force vs. palpation depth can be used to map the relative stiffness of the tissue. Next the boundaries are traced by thresholding this stiffness map, enabling a better understanding of tumor size and location. This approach can clearly distinguish both tumors as well as some macroscopic tumor features.

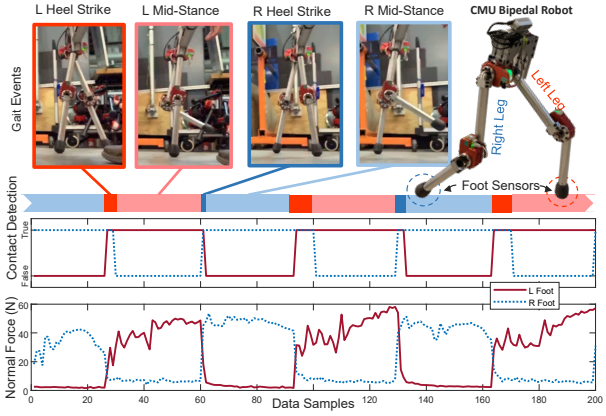

Fig. 3: Foot Sensor for contact force measurement and real-time gait events detection, under heavy impact conditions.

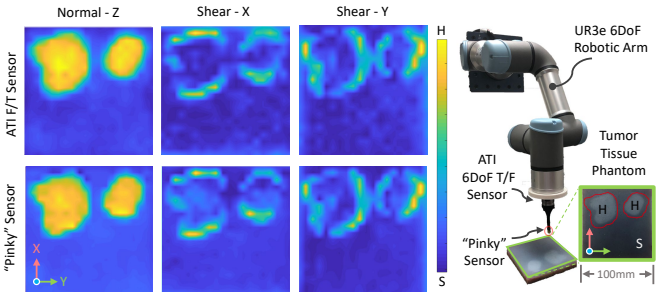

Fig. 4: 3D Stiffness estimation and result comparison (along normal and shear direction) over a tumor tissue phantom using the ATI and "Pinky" Sensor (H - Hard Tumor, S - Soft tissue).

IV. Conclusion and Discussion

We presented a generalizable model and design for a highly tunable embedded magnet tactile sensors. To demonstrate its versatility, we designed and manufactured two different versions of the proposed sensor: a highly accurate small form factor version which demonstrates the sensitivity and scalability of this design and a larger foot sensor which demonstrates the durability of the design under the high impact of robotic locomotion. These sensors demonstrate the breadth of possible designs as well as how changing small parameters can be used to tune their range and resolution for a wide variety of custom applications.

Acknowledgment

The authors would like to thank Xinyu Wang, Steve Crews and Zixin Zhang. And this work was partially supported by the CMU Manufacturing Futures Initiative (MFI). [1]

[1] sup. materials https://youtu.be/eKHvWxwSocM
https://www.ri.cmu.edu/project/robotic-force-sensor-and-perception/

REFERENCES

[1] J. W. James, N. Pestell, and N. F. Lepora, "Slip detection with a biomimetic tactile sensor," *IEEE Robotics and Automation Letters*, vol. 3, no. 4, pp. 3340–3346, 2018.

[2] Z. Su, K. Hausman, Y. Chebotar, A. Molchanov, G. E. Loeb, G. S. Sukhatme, and S. Schaal, "Force estimation and slip detection/classification for grip control using a biomimetic tactile sensor," in *2015 IEEE-RAS 15th International Conference on Humanoid Robots (Humanoids)*, 2015, pp. 297–303.

[3] W. Yuan, R. Li, M. A. Srinivasan, and E. H. Adelson, "Measurement of shear and slip with a gelsight tactile sensor," in *2015 IEEE International Conference on Robotics and Automation (ICRA)*, 2015, pp. 304–311.

[4] J. Li, S. Dong, and E. Adelson, "Slip detection with combined tactile and visual information," in *2018 IEEE International Conference on Robotics and Automation (ICRA)*, 2018, pp. 7772–7777.

[5] H. Wang, G. De Boer, J. Kow, A. Alazmani, M. Ghajari, R. Hewson, and P. Culmer, "Design methodology for magnetic field-based soft tri-axis tactile sensors," *Sensors*, vol. 16, no. 9, 2016. [Online]. Available: https://www.mdpi.com/1424-8220/16/9/1356

[6] D. J. Griffiths, *Introduction to electrodynamics; 4th ed.* Boston, MA: Pearson, 2013, re-published by Cambridge University Press in 2017. [Online]. Available: https://cds.cern.ch/record/1492149

[7] H. Brinson and L. Brinson, *Polymer engineering science and viscoelasticity: An introduction, Second edition*. Springer US, Jan. 2015, pp. 1–482.

[8] N. Kumar, O. Piccin, L. Meylheuc, L. Barbé, and B. Bayle, "Design and modeling of a polymer force sensor," *IEEE/ASME Transactions on Mechatronics*, vol. 21, no. 1, pp. 555–564, 2016.

[9] G. Valsecchi, R. Grandia, and M. Hutter, "Quadrupedal locomotion on uneven terrain with sensorized feet," *IEEE Robotics and Automation Letters*, vol. 5, no. 2, pp. 1548–1555, 2020.

[10] S. Crews, "Unified foothold selection and motion planning for legged systems in real-time over rough terrain," Ph.D. dissertation, Carnegie Mellon University, 2020.

[11] R. S. Dahiya, G. Metta, M. Valle, and G. Sandini, "Tactile sensing—from humans to humanoids," *IEEE Transactions on Robotics*, vol. 26, no. 1, pp. 1–20, 2010.

[12] J. Palep, "Robotic assisted minimally invasive surgery," *Journal of minimal access surgery*, vol. 5, pp. 1–7, 02 2009.

[13] E. Ayvali, A. Ansari, L. Wang, N. Simaan, and H. Choset, "Utility-guided palpation for locating tissue abnormalities," *IEEE Robotics and Automation Letters*, vol. 2, no. 2, pp. 864–871, 2017.